Nat. Hazards Earth Syst. Sci., 13, 3479–3492, 2013
www.nat-hazards-earth-syst-sci.net/13/3479/2013/
doi:10.5194/nhess-13-3479-2013

Natural Hazards and Earth System Sciences
Open Access

Validation study of TMPA 3B42V6 in a typical alpine and gorge region: Jinsha River basin, China

Y. C. Yang[1,2,3], G. W. Cheng[1], J. H. Fan[1], W. P. Li[1,2,4], J. Sun[1,2], and Y. K. Sha[1,2]

[1]The Key Laboratory of Mountain Environment Evolution and its Regulation,
Institute of Mountain Hazards and Environment, University of Chinese Academy of Sciences, Chengdu 610041, China
[2]University of Chinese Academy of Sciences, Beijing 100049, China
[3]College of Civil Engineering and Architecture, Guangxi University, Nanning 530004, China
[4]Land and Resource College, China West Normal University, Nanchong 637002, China

Correspondence to: G. W. Cheng (gwcheng@imde.ac.cn)

Received: 6 November 2012 – Published in Nat. Hazards Earth Syst. Sci. Discuss.: –
Revised: 4 August 2013 – Accepted: 7 August 2013 – Published: 23 December 2013

Abstract. Because of density and distribution flaws inherent with in situ rainfall measurements, satellite-based rainfall products, especially the Tropical Rainfall Measuring Mission (TRMM), were expected to offer an alternative or complement for modeling of hydrological processes and water balance analysis. This study aims at evaluating the validity of a standard product, the TRMM Multi-satellite Precipitation Analysis (TMPA) 3B42V6, by comparing it with in situ ground gauge datasets on a typical alpine and gorge region in China, the Jinsha River basin. The validation study involved the performance of the 3B42V6 product on 3 h, daily and monthly temporal scales. Statistical analysis methods were used for rainfall and rain event estimation. The results affirmed that the 3B42V6 product demonstrated increasing accuracy when the temporal scales were increased from 3 h to daily to monthly. The mean correlation coefficient of rainfall time series between the 3B42V6 product and the gauge over the Jinsha River basin reached 0.34 on the 3 h scale, 0.59 on the daily scale, and 0.90 on the monthly scale. The mean probability of detection (POD) of the 3B42V6 product reached 0.34 on the 3 h scale and 0.63 on the daily scale. The 3B42V6 product of 80.4 % of stations obtained an acceptable bias (± 25 %) over the investigation area. A threshold of nearly 5.0 mm d^{-1} in daily rainfall intensity split the 3B42V6 product into overestimates (< 5.0 mm d^{-1}) and underestimates (> 5.0 mm d^{-1}). The terrain elements of altitude, longitude, and latitude were the major influencing factors for 3B42V6 performance. In brief, the 3B42V6 dataset has great potential for research on hydrologic processes, especially daily or large temporal scale. As for fine temporal scale applications, such as flood predictions based on a 3 h scale dataset, it is necessary to conduct adjustments or to combine the 3B42V6 product with gauges to be more accurate regarding the issues in the study area or in analogous regions with complicated terrains.

1 Introduction

Rainfall is the most important atmospheric input to land surface hydrology models. Therefore, accurate rainfall inputs with fine spatio-temporal resolution are essential for reliable hydrologic predictions (Sorooshian et al., 2005). However, it is also one of the most difficult atmospheric inputs to measure, in part because there is a large inherent variation in rainfall. Additionally, ground-based rainfall measurements are either sparse or nonexistent in many remote parts of the world, particularly in developing countries. Finally, there are high costs associated with the establishment and maintenance of the necessary infrastructure. These limitations are all true for the Jinsha River basin, which is connected to the upper reaches of the Yangtze River in China (Fig. 1). Satellite-based rainfall estimates with high spatio-temporal resolution and large aerial coverage provide a potential alternative source of forcing data for hydrological models in regions where conventional in situ rainfall measurements are not readily available (Su et al., 2008). Nevertheless, a validation study of satellite-based rainfall estimates, either as

a complement or alternative for in situ gauge rainfall, is a high priority for hydrology and ecology research. The Jinsha River basin in western China is a typical alpine and gorge terrain and provides a prime location for a case study regarding the adequacy of satellite-derived rainfall.

There are now at least 12 distinct satellite rainfall products available (Ebert et al., 2007). The primary trend in the development of satellite rainfall products is the move toward merged datasets that take advantage of the best available data (Tobin and Bennett, 2010). Thus far, satellite-based products from National Aeronautics and Space Administration (NASA), the Tropical Rainfall Measuring Mission (TRMM) Multi-satellite Precipitation Analysis (TMPA) (Huffman et al., 2007) have been widely applied in hydrological processes, meteorology, and ecology (Jia et al., 2011). For instance, the TMPA 3B42 version 6 product, referred to in this paper as the 3B42V6, was based on the combination of passive microwave (PMW) and infrared (IR) precipitation estimates from all available satellites. It utilized PMW-calibrated IR-based rainfall estimates to fill in the PMW coverage gaps (Huffman et al., 2007). The 3B42V6 performed well compared with other satellite-based rainfall products, an apparent good match for the frequency of rainy events, but a weaker match for the amount of precipitation over four African river basins (Zambezi, Volta, Juba-Shabelle, and Baro-Akobo) (Vera et al., 2012). These findings have also been confirmed over Uganda (Asadullah et al., 2008).

As one of the standard TMPA mainstream products, the 3B42V6 was compared with gauge data from different Asian countries, including India (Brown, 2006), Thailand (Chokngamwong et al., 2008), Bangladesh (Islam and Uyeda, 2007), and Nepal (Islam et al., 2010). These studies illustrated that discrepancies existed between the 3B42V6 and the gauge data on the daily scale. However, the two datasets showed a stronger correlation and rain event detection in a monthly comparison (Mansour, 2011). Similar work had been done in several regions of China, such as the Tibetan Plateau (Chen et al., 2012), the Yangtze River basin (Gu et al., 2010), Poyang Lake (Li et al., 2012), eastern China (Yuan et al., 2012), and China in its entirety (Zhou et al., 2008; Liu et al., 2011; Luo et al., 2011). Reasonable spatial distribution and acceptable error magnitude of the 3B42V6 were also confirmed on the daily or greater temporal scales.

However, these studies were fairly short in terms of hourly scale and few validated data from regions with complex terrain. This is important for the employment of the 3B42V6 in the research on hydrological processes, especially in flood prediction. Additionally, discrepancies of the 3B42V6 and gauged rainfall for different rainfall intensities would provide useful information regarding the application of 3B42V6. Overall, this research is aimed to validate the 3B42V6 and its use in the research on hydrologic processes in the Jinsha River basin. Specifically, this work involved 3 h, daily, and monthly scale validations of the 3B42V6, and mainly focused on rainfall amount estimates, errors in seasonal differences, rain event detection, accuracy in different rainfall intensities, and the influence of the terrain (Sect. 3). Subsequently, imperative discussions for the consistencies or discrepancies of the two datasets are given (Sect. 4). The conclusion summarizes the opinion as to whether the 3B42V6 can be applied in the research of hydrological processes (Sect. 5).

2 Investigation area, data, and methodology

2.1 Investigation area

The Jinsha River basin is a typical watershed with alpine and gorge terrain connected to the upper reaches of the Yangtze River in China (Fig. 1). Its area is about 13.2×10^4 km^2, ranging in height from 263 m to 5910 m. Complicated climate changes and frequent rainfall, occurring with high intensity but of short duration, are primary characteristics in the region, which often leads to flooding of the Three Gorges Dam reservoir (Shen and Yang, 2007). Therefore, a satellite-based rainfall dataset with a higher spatio-temporal resolution would contribute to a more precise stream flow modeling or prediction, which would be significant for the operation and management of the Three Gorges Dam reservoir.

2.2 Data

2.2.1 Ground rainfall gauge dataset

The dataset used for validation was comprised of 107 rain gauge stations distributed over the investigation area (Fig. 1). The ground rainfall gauge dataset are derived from the Water Regime Database belonging to the Three Gorges Cascaded Hydropower Scheduling Center. The time periods of the gauge data selected in this study run from 1 January 2008 to 31 December 2010, expressed in Beijing time (UTC+8 h), where UTC is the universal coordinated time. Data were obtained every three hours during these days at 02:00, 05:00, 08:00, 11:00, 14:00, 17:00, 20:00 and 23:00 from the gauge dataset on Beijing time.

2.2.2 TMPA dataset

Based on calibration by the TRMM Microwave Imager (TMI) rainfall products and the TRMM Combined Instrument (TCI), TMPA has been computed for two products: real time (RT) (January 2002 to present) and post-processed (January 1998 to present) (Su et al., 2008). The post-processed product was used to develop the version 6 algorithm, referred to as the 3B42V6. Huffman et al. (2007) presented that the RT product uses TMI rainfall as the calibrator, while the 3B42V6 uses the TCI, which is considered superior but exhibits a 10–15 day lag in real time. Research done by Yong et al. (2010) in China's Laohahe Basin showed that the 3B42RT data have almost no hydrologic utility, even on a monthly scale. In contrast, the 3B42V6 data can produce superior

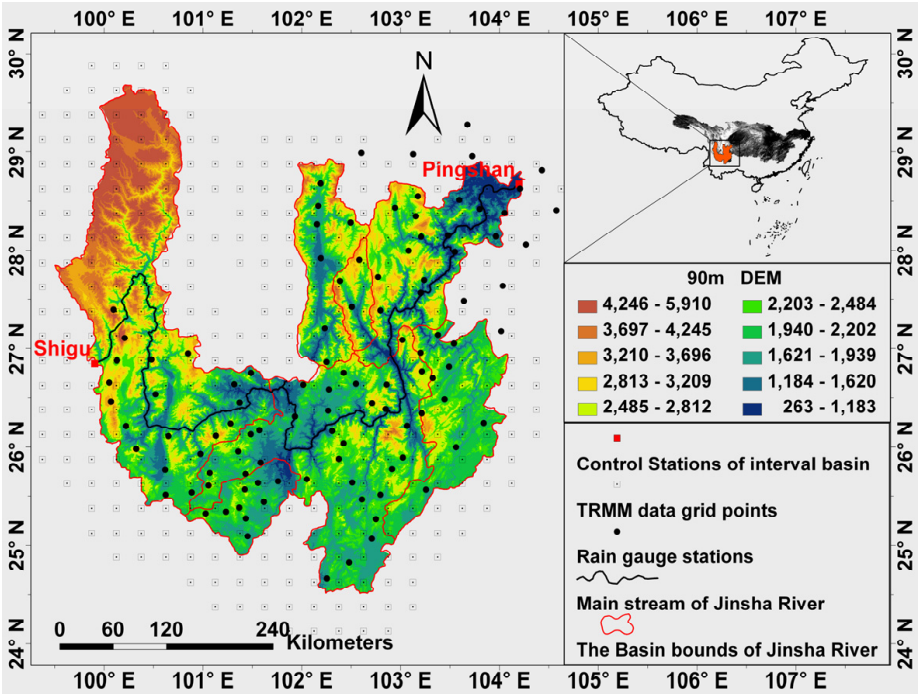

Fig. 1. The distribution of gauged rainfall stations (107 stations) and TMPA 3B42V6 grids (393 grids) in Jinsha River basin. The 90 m Digital Elevation Model (DEM) dataset was downloaded from http://datamirror.csdb.cn.

hydrologic predictions with reduced error propagation from input to stream flow on both daily and monthly scales. Taking into account the complex terrain and the fact that data needed to be collected every three hours in the investigation area, the 3B42V6 product became the product selected for this study. The 3B42V6 provides rainfall estimates on a 3 h temporal scale, in $0.25° \times 0.25°$ latitude-longitude resolution covering the globe between the latitude band of 50°N/S and can be downloaded for free at http://trmm.gsfc.nasa.gov. The selected periods of the 3B42V6 are from 31 December 2007, 18:00 to 31 December 2010, 15:00, expressed by UTC and covered by one tile of $0.25° \times 0.25°$. This correlates to an area of approximately 25 km × 25 km in the Jinsha River basin (Fig. 1). There are eight 3 h steps over a day (00:00, 03:00, 06:00, 09:00, 12:00, 15:00, 18:00, and 21:00) in this dataset by UTC. In order to be compared with the rainfall gauge dataset mentioned in Sect. 2.2.1, the 3B42V6 dataset was converted to the Beijing time series using UTC+8 h, corresponding to the rainfall gauge dataset collected from 1 January 2008 to 31 December 2010 at 02:00, 05:00, 08:00, 11:00, 14:00, 17:00, 20:00 and 23:00 each day in Beijing time.

2.3 Methodology and indices

2.3.1 Methodology

For day and month periods, both datasets were summarized in a time series of daily and monthly scales from every ground station (107 stations) and 3B42V6 grid (393 grids). The gauge data for each station was manually checked for quality and represented the "truth" for the nearest 3B42V6 grid (107 grids corresponding to ground stations).

A validation study of the 3B42V6 guidelines covered (1) sum rainfall consistency (Sect. 3.1), (2) temporal correlation (Sect. 3.2), (3) spatial correlation (Sect. 3.3), (4) rainfall relative bias (Sect. 3.4), (5) rain event detection (Sect. 3.5), (6) accuracy at different gauged daily rainfall intensities (Sect. 3.6), and (7) terrain influence (Sect. 3.7). The related statistical analysis and rain event estimation methods were used. Spatial patterns of rainfall (393 grids vs. 107 stations) or related indices (107 grids vs. 107 stations) were generated by the inverse distance weighted (IDW) interpolation method, selected for its simplicity and ease of execution. Statistical analysis methods were presented to validate the consistencies and discrepancies between the 3B42V6 and gauges rainfall in the investigation area.

2.3.2 Validation statistical indices

Several validation statistical indices were used, and their computational formulas are shown in Table 1. The standard deviation (STDEV) depicted general discrepancies of the two datasets. The Pearson correlation coefficient (CC) was used to validate the time series (TCC) and spatial patterns (SCC) of the degree of agreement between the 3B42V6 and the gauged rainfall. The Nash–Sutcliffe coefficient of efficiency (NSE) evaluated the comprehensive fitting degree of consistency of the time series of the datasets. As to rainfall amount deviation, the relative bias (BIAS) was adequate to describe the systematic bias. For a convenient comparison to a related study (Scheel et al., 2011), the selected mean error (ME) explained the average difference between the 3B42V6 and the gauged rainfall with the augmentation of gauged daily rainfall intensity. With regard to rain event detection, the frequency bias index (FBI) expresses the ratio of 3B42V6 to the gauged rain events. A value of FBI above 1.0 implies that the 3B42V6 overestimated the number of rain events in the investigation period, while below 1.0 implies its underestimation. The probability of detection (POD) quantifies the fraction of rain events that were correctly estimated by the 3B42V6 to the total number of the gauged rain events. The critical success index (CSI) examined the correspondence between the 3B42V6 and gauged occurrence of rain events (Ebert et al., 2007; Yong et al., 2010; Scheel et al., 2011; Montero-Martínez et al., 2012).

The performance of the 3B42V6 by BIAS was characterized into three basic categories (Brown, 2006): underestimates ($> 10\,\%$), overestimates ($< -10\,\%$) and approximately equal ($\pm 10\,\%$) in different seasons, and expanded acceptable accuracy ($\pm 25\,\%$). In addition, two threshold values of $1.0\,\mathrm{mm\,d^{-1}}$ for the daily scale and $0.3\,\mathrm{mm\,3\,h^{-1}}$ for the 3 h scale were used in computing the following indices: FBI, POD, and CSI. The classification of daily rainfall intensity of the two datasets also adopted a $1.0\,\mathrm{mm\,d^{-1}}$ threshold value. It is generally acknowledged that less than $1.0\,\mathrm{mm\,d^{-1}}$ ($0.3\,\mathrm{mm\,3\,h^{-1}}$) is regarded as invalid rainfall in a day (3 h period) (Dai et al., 2007; Yong et al., 2010; Mansour, 2011; Scheel et al., 2011).

3 Results and analysis

3.1 Sum rainfall consistency of the 3B42V6 against the gauged dataset

Mean rainfall time series of the gauged dataset and the 3B42V6 from 2008 to 2010 on 3 h, daily, and monthly scales were collected from 107 stations and the nearest corresponding grids of 3B42V6. The statistical indices of total rainfall (TR), mean rainfall (MR) and STDEV were then computed and are shown in Fig. 2. There was approximately 0.2 % relative bias for the TR between the two datasets in the three

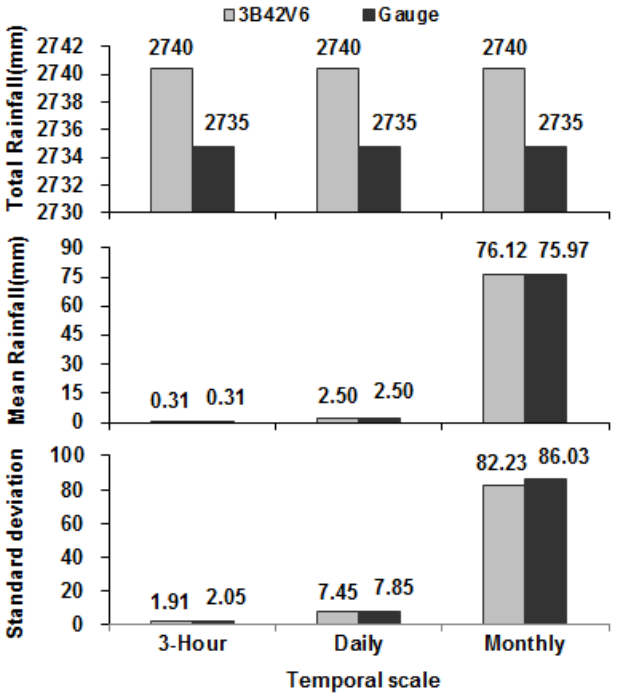

Fig. 2. Two-dimensional histograms of statistics comparisons between gauge and 3B42V6 on sum rainfall, mean rainfall, and standard deviation on 3 h, daily and monthly scales. These two mean rainfalls were averaged gauged rainfall over 107 stations and correspondingly the nearest 107 3B42V6 grids' rainfall over 2008–2010, respectively.

temporal scales for the same source datasets derived from the 3 h scale. The MR and STDEV values for the 3B42V6 and the gauged rainfall were almost the same for the three temporal scales. These results indicate an attractive consistency in sum rainfall amount of the 3B42V6 and the gauged dataset in the investigation area.

The consistency of the two datasets regarding mean rainfall time series on different temporal scales was examined. For the 3 h and daily scales, time periods from May to October (averaging three years) were selected. For the monthly scale, the whole period from 2008 to 2010 was selected. The mean rainfall time series fitting curves are shown in Fig. 3. It was clear that the degree of mean rainfall agreement gradually improved as the temporal scales increased by TCC from 0.53 (3 h) to 0.81 (daily) to 0.99 (monthly). These were acquired through the test of 99 % significance test level with the critical correlation coefficient (Ccc) of 0.07 (3 h, derived from 8768 sample numbers), 0.19 (daily, derived from 1096 sample numbers), and 0.41 (monthly, derived from 36 sample numbers). The synchronous changing of NSE values was from 0.03 (3 h) to 0.56 (daily) to 0.98 (monthly). However, when compared to the TCC value, the low NSE value on the 3 h scale indicated that significant

Table 1. The validation statistical indices used to compare the TMPA 3B42V6 and the rainfall gauge data*.

Statistical index	Unit	Equation	Value range	Perfect value
Standard deviation (STDEV)	mm	$\mathrm{STDEV} = \sqrt{\frac{\sum_{i=1}^{n}(R_i-\bar{R})^2}{(n-1)}}$	$[0,+\infty)$	0
Correlation coefficient (CC)	NA	$\mathrm{CC} = \frac{\sum_{i=1}^{n}(G_i-\bar{G})(T_i-\bar{T})}{\sqrt{\sum_{i=1}^{n}(G_i-\bar{G})^2}\cdot\sqrt{\sum_{i=1}^{n}(T_i-\bar{T})^2}}$	$[-1,1]$	1
Nash–Sutcliffe coefficient efficiency (NSE)	NA	$\mathrm{NSE} = 1 - \frac{\sum_{i=1}^{n}(T_i-G_i)^2}{\sum_{i=1}^{n}(G_i-\bar{G})^2}$	$(-\infty,1]$	1
Relative bias (BIAS)	%	$\mathrm{BIAS} = \frac{\sum_{i=1}^{n}(G_i-T_i)}{\sum_{i=1}^{n}G_i}\times 100\,\%$	$(-\infty,+\infty)$	0
Mean error (ME)	mm	$\mathrm{ME} = \frac{1}{n}\sum_{i=1}^{n}(T_i - G_i)$	$(-\infty,+\infty)$	0
Frequency bias index (FBI)	NA	$\mathrm{FBI} = (H+F)/(H+M)$	$[0,+\infty)$	1
Probability of detection (POD)	NA	$\mathrm{POD} = H/(H+M)$	$[0,1]$	1
Critical success index (CSI)	NA	$\mathrm{CSI} = H/(H+M+F)$	[0,1]	1

* Notation: n, number of samples; R_i, rainfall time series; $\bar{R}$, mean rainfall; T_i, satellite-based precipitation (TMPA 3B42V6); G_i, gauged rainfall; H, gauged rain correctly detected; M, gauged rain not detected; F, rain detected but not gauged; N, no rain detected and no rain gauged (for the above indices, CC, NSE, BIAS and ME, refer to Yong et al. (2010); for FBI, POD and CSI, refer to Ebert et al. (2007), Scheel et al. (2011) and Montero-Martínez et al. (2012), for a detailed explanation).

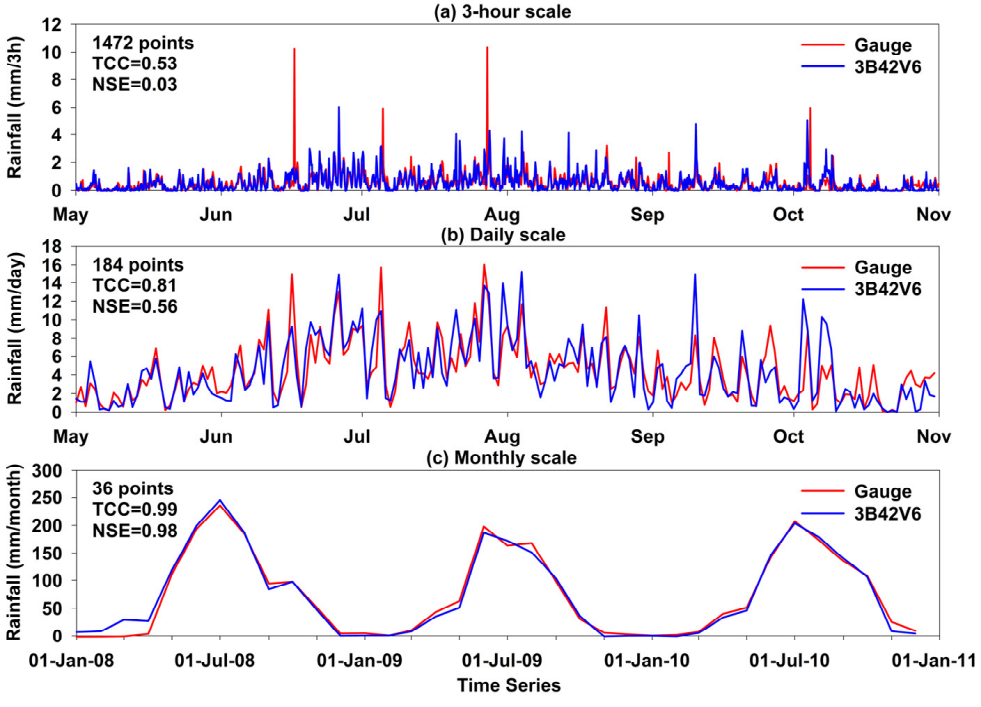

Fig. 3. Comparison curves of mean rainfall time series between the 3B42V6 (107 grids) and the gauges (107 stations). These two mean rainfall time series were calculated the same as in Fig. 2 on the monthly scale, but selected periods – May to October (wet season) from 2008, 2009 and 2010, and then the rainfall series of those three years – were averaged on the 3 h and daily scales.

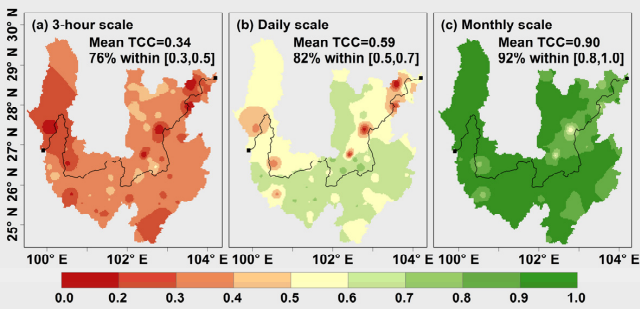

Fig. 4. Spatial patterns of temporal correlation coefficients between the 3B42V6 (107 grids) and the gauges (107 stations) on 3 h **(a)**, daily **(b)**, and monthly **(c)** scales by the IDW interpolation method.

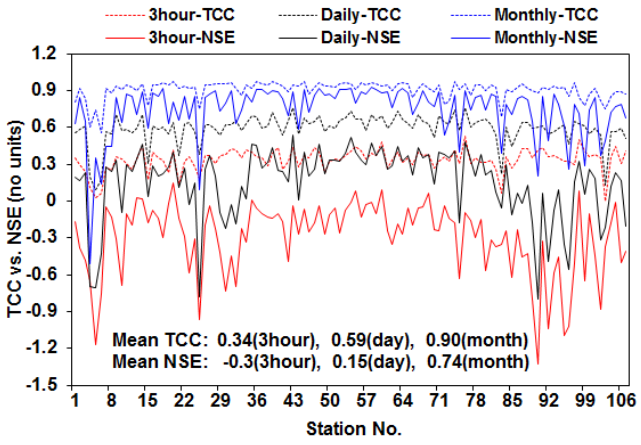

Fig. 5. Compared curves of the temporal correlation coefficient (TCC) versus the Nash–Sutcliffe coefficient of efficiency (NSE) between the 3B42V6 (107 grids) and the gauges (107 stations) for the three temporal scales over 2008-02010.

mean rainfall amount differences existed in its mean rainfall time series. The daily scale, however, demonstrates acceptable mean rainfall amount discrepancies. These phenomena did not appear on the monthly scale because of approximately equal values of the TCC and NSE.

3.2 Temporal correlation between 3B42V6 and gauged rainfall

For further examination of the consistency in single station, rainfall time series of gauges from 107 stations and of the 3B42V6 from the nearest corresponding grids over 2008–2010 were validated by TCC and NSE at the three temporal scales (Figs. 4 and 5). Figure 4 shows 107 points of TCC spatial patterns from the two datasets using the IDW interpolation method. The main variation ranges of TCC were 0.3–0.5 (76 % points, 3 h), 0.5–0.7 (82 % points, daily) and 0.8–1.0 (92 % points, monthly), with exception of local regions. The mean values of TCC over the region were 0.34 (3 h), 0.59 (daily), and 0.90 (monthly). Overall, the TCC values displayed similar patterns among the three temporal scales but demonstrated successive growth with augmentation of the temporal scales. There were no notable distribution characteristics in any of the TCC spatial patterns.

Figure 5 shows the variations of TCC and the corresponding NSE values belonging to the 107 points between the two datasets. There were synchronized variation trends of the two index values among the three temporal scales, with exception of local differences between TCC and NSE. The mean values of NSE in Fig. 5 indicate a good fitting degree of consistency on the monthly scale (mean NSE = 0.74), but not on the daily (mean NSE = 0.15) and the 3 h (mean NSE = −0.3) scales. This illustrates notable discrepancies of rainfall amounts of single stations on the daily and the 3 h temporal scales.

3.3 Spatial correlation between 3B42V6 and gauged rainfall

The spatial correlation of rainfall amounts plays an important role on average surface rainfall calculations in the research of hydrologic processes, especially in hydrological modeling and prediction. It was proposed by Buarque et al. (2011) and Clarke et al. (2011) that unless the spatial correlations had been considered, uncertainty in rainfall characteristics would exist in differences between values obtained from alternative datasets. Therefore, it is still necessary to validate the 3B42V6 against gauges in spatial consistency.

Figure 6 displays spatial pattern comparisons of the 3B42V6 against gauged rainfall in typical time intervals of the three temporal scales using the IDW interpolation method. All comparisons were made through the 95 % significance test level using a Ccc of 0.19, which was derived from 107 sample numbers. The exception is the 3 h scale in 2008, which was tested through the 90 % significance test level (Ccc = 0.16). On the whole, the spatial distribution characteristics of the two datasets agreed with each other, and there was no significant SCC superiority among the three temporal scales. For example, the maximum value of the SCC in 2008 was on the daily scale (SCC = 0.53); however, in 2009 it was on the 3 h scale (SCC = 0.71). Conversely, in 2010 the maximum value of SCC was on the monthly scale (SCC = 0.40). Of course, these typical time intervals were selected by subjective experience with heavy rainfall amounts in 3 h, daily and monthly periods.

The SCC of the three temporal scales from the sample numbers of 107 stations and corresponding 107 grids in the two datasets was computed and averaged for each month (Fig. 7). Figure 7 indicates that valid SCC values of the three temporal scales, which were through the 95 % significance test level, were mainly concentrated in heavy rainfall months from May to September (shown in blue). Invalid SCC values of the three temporal scales, which were not through the 95 % significance test level, were mainly gathered in light rainfall months (shown in red). It is noteworthy that the valid

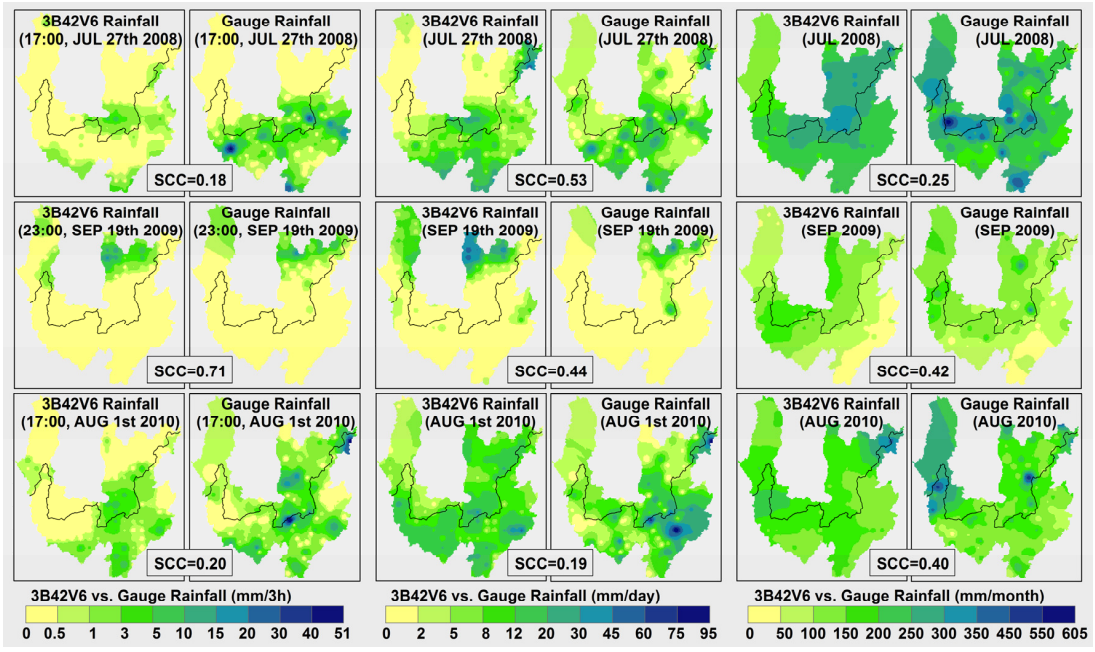

Fig. 6. Rainfall pattern comparisons of the 3B42V6 (393 grids) against the gauges (107 stations) in the typical time intervals of the three temporal scales by the IDW interpolation method.

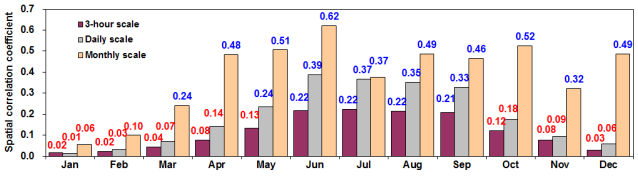

Fig. 7. The two-dimensional histograms of the spatial correlation coefficient discrepancies with monthly variations between the 3B42V6 (107 grids) and gauges (107 stations) for the three temporal scales; each value is the average of all time interval values of its month. The red numbers indicated the SCC were not through the 95 % significance test and the blue numbers demonstrated the SCC were through the 95 % significance test.

SCC values of monthly scale were emerged almost whole year except individual months, such as January and February. The jump in SCC values from December to January on the monthly scale was partly attributed to uncertainty, which was partly derived from 3B42V6 detectability in slight rainfall, and partly attributed to monthly rainfall that was summed up from daily or 3 h rainfall and averaged, and partly ascribed to sample values as only three months, and partly ascribed to sample values as only three months.

Furthermore, the variation trends over time of the SCC were illustrated from June to August for three years on the 3 h and daily scales, but for the whole period from 2008 to 2010 on the monthly scale (shown in Fig. 8). The missing values of SCC existed on the 3 h scale because of zero rainfall at all of the 107 stations from either the gauges or the 3B42V6 during that time interval. There was no significant agreement amongst the SCC values on the 3 h or daily scale over the three years, due to the high spatio-temporal variability of rainfall. In general, the mean SCC values successively increased as the temporal scales were augmented. However, the high SCC values of heavy rainfall time intervals on 3 h and daily scales were not less or even greater than many SCC values of monthly scale. Of course, there are more near zero or even negative SCC values on 3 h and daily scales than on the monthly scale.

3.4 Seasonal differences between 3B42V6 and gauged rainfall shown by relative bias

The relative bias of the 3B42V6 against the gauged rainfall time series during 2008 to 2010 was calculated. The spatial pattern and seasonal differences of BIAS were given in Figs. 8 and 9. It should be mentioned that the bias computational formula (Table 1) represents the relative bias of the sum rainfall amount; thus there was an identical same bias value for each station among the 3 h, daily, or monthly scales over all of the time periods. They are not distinguished and also not identified on the temporal scale in this study.

The spatial pattern of BIAS shown in Fig. 8 indicated that acceptable accuracy (± 25 %) of the 3B42V6 dominated, and there are no obvious regular spatial distributions of over-/underestimates in several local areas. The mean BIAS value of the entire area was presented as 3.94 %, which indicated a slight overestimation of the 3B42V6 against gauges

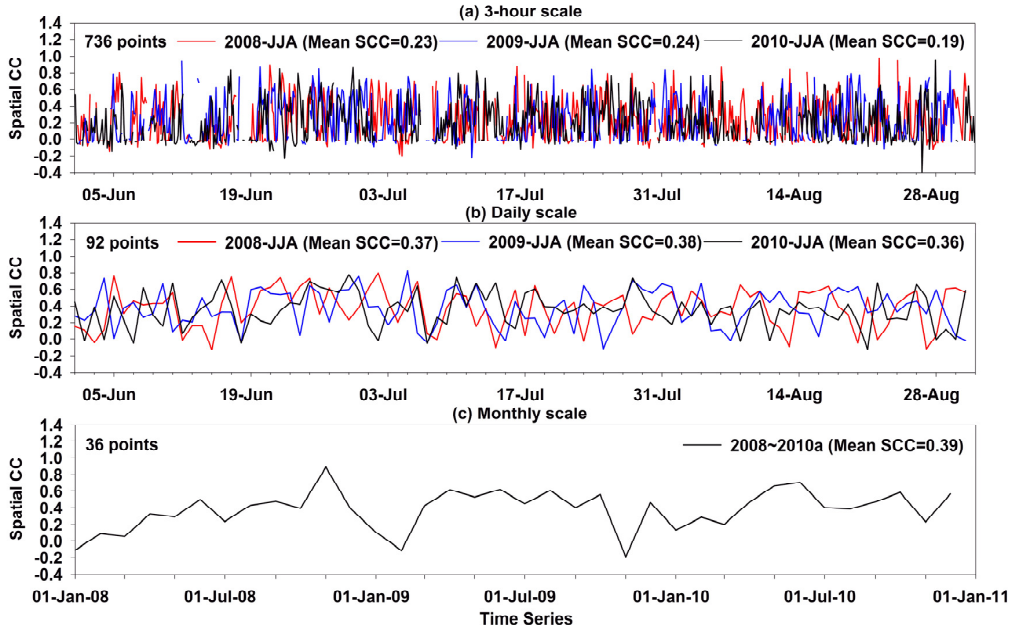

Fig. 8. Variable curves of the spatial correlation coefficient between the 3B42V6 (107 grids) and the gauges (107 stations): June to August of 2008–2010 on 3 h **(a)** and daily **(b)** scales, but the whole period over 2008–2010 on the monthly scale **(c)**.

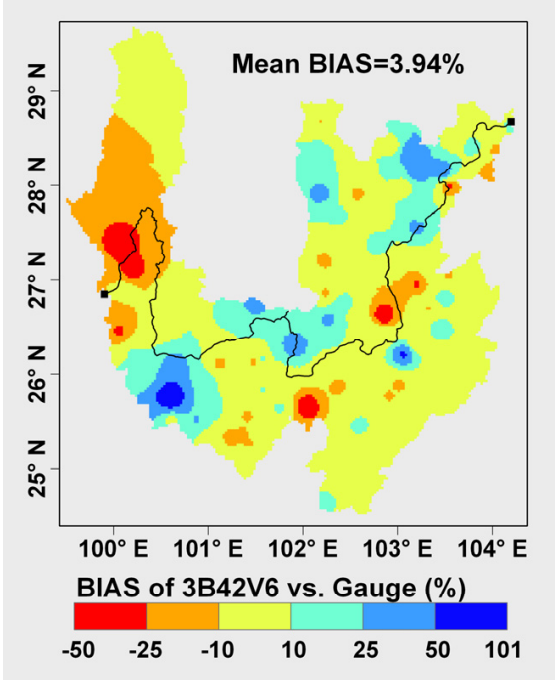

Fig. 9. BIAS spatial pattern calculated from the 3B42V6 (107 grids) against the gauged rainfall time series (107 stations) over 2008–2010, interpolated by the IDW interpolation method.

for the total rainfall amount. Moreover, the BIAS levels shown in Fig. 9 displayed that the 3B42V6 estimates approximately equal (± 10 %) to gauged rainfall reached 37.4 %, acceptable accuracy (± 25 %) achieved 80.4 %, overestimates obtained 36.4 %, and underestimates attained 26.2 % over 2008–2010. As to different seasons, the 3B42V6 estimate of acceptable accuracy in winter (DJF) was significantly less than other seasons or the whole period. Conversely, the 3B42V6 estimates of overestimates (> 10 %) and underestimates (< 10 %) in winter (DJF) were greater than the other seasons or the whole period. The 3B42V6 has a similar estimated accuracy of BIAS levels amongst the wet seasons (JJA and SON) and the whole period. Nevertheless, the 3B42V6 has greater overestimates but less approximately equal and acceptable accuracy of BIAS in the dry seasons (DJF and MAM) than in the whole period. Overall, the overestimates of 3B42V6 were greater than the underestimates in different seasons.

3.5 Rain event detection ability of the 3B42V6

The rain event detection ability of the 3B42V6 can be validated by the FBI, POD and CSI indices, introduced in Sect. 2.3.2. These indices were computed on both the 3 h and daily scales with a threshold also mentioned in Sect. 2.3.2. Their spatial patterns were also interpolated using the IDW method (Fig. 10). The patterns of FBI, POD and CSI shown in Fig. 10 indicated that there were no obvious regular spatial distributions of them, especially in FBI and POD. The mean values of them on the daily scale, as FBI = 1.05,

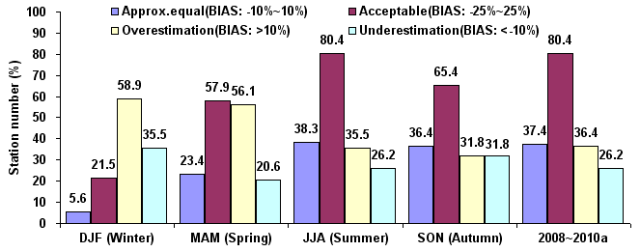

Fig. 10. The two-dimensional histograms of station number percentages divided by BIAS value ranges from 107 stations; where BIAS was computed the same as in Fig. 8 but for different time periods.

POD = 0.63, and CSI = 0.44, were greater than on the 3 h scale, as FBI = 0.86, POD = 0.34, and CSI = 0.22. The mean value of FBI demonstrated that the 3B42V6 slightly overestimates rain events on the daily scale, but underestimates rain events on the 3 h scale. Specifically, the value of FBI on 3 h scale displayed greater than 1.0 in the upper reaches but less than 1.0 in the lower reaches of the Jinsha River basin. However, the values of FBI on daily scale were almost all greater than 1.0 over the region.

For the sake of better understanding the variation trends of the performance of 3B42V6 on rain event detection on different temporal scales, the FBI, POD, and CSI curves are given in Fig. 11, corresponding to patterns shown in Fig. 10. The curves of these indices shown in Fig. 11 displayed significant synchronous variation of pair indices between 3 h and daily scales, which have the similar results as Fig. 11 shown by SCC values of 0.94 (FBI), 0.95 (POD) and 0.91 (CSI) between the two temporal scales. The rain event detection ability of 3B42V6 on the daily scale was greater than on the 3 h scale.

3.6 3B42V6 performance with augmentation of gauged daily rainfall intensity

Primarily, the gauged daily rainfall intensity was divided into 10 classifications: 0, 0–0.5, 0.5–1, 1–2, 2–5, 5–10, 10–20, 20–30, 30–50 and $> 50\,\mathrm{mm\,d^{-1}}$. The 3B42V6 rainfall time series fell into the ten classifications of the gauged daily rainfall intensity. The indices of TCC, ME and POD of the 3B42V6 against the gauged rainfall time series in the ten classifications of gauged daily rainfall intensity were calculated and averaged from data of 107 stations. The variation trends of these indices with the gauged daily rainfall intensity are shown in Fig. 12. Regarding rainfall time series agreement, the value of TCC between the 3B42V6 and the gauged rainfall represented a gradual increase with the augmentation of gauged daily rainfall intensity, even though fluctuation existed. The value of POD significantly improved with the increase of gauged daily rainfall intensity from 0 to $> 50\,\mathrm{mm\,d^{-1}}$. Inversely, the value of ME gradually decreased from a small positive value to large negative value when augmented with gauged daily rainfall intensity. It was easy to know that there was a threshold of daily rainfall intensity slightly below $5.0\,\mathrm{mm\,d^{-1}}$, which split the 3B42V6 rainfall into overestimation of greater than $5.0\,\mathrm{mm\,d^{-1}}$ and underestimation of less than $5.0\,\mathrm{mm\,d^{-1}}$.

3.7 Influence of terrain on 3B42V6 performance

The influence of terrain gives rise to the high spatio-temporal variability of rainfall. This is especially true in mountainous regions, such as the Jinsha River basin which has alpine and gorge terrains. Therefore, the influence of terrain on the 3B42V6 performance in this investigation area should be considered. Influence factors of the altitude, longitude, latitude, slope, and the aspect of each station were usually selected to evaluate the geographical factors on the impact of rainfall, and so these were taken into account in this study. Actually, it is an indirect method to validate the variation trends of statistical indices between the two datasets with these geographical factors, which is intended to reflect the performance of 3B42V6 affected by the degree of these factors. It is worth mentioning that the study area has complex terrain and is located in the west of Sichuan Basin, which influenced the systematic climate zone changes. That is why the altitude, longitude and latitude were selected. In addition, although the slope and aspect are local, regime-dependent factors, they were also taken into account just for integrity of analysis. In order to determine the main influence factors on the performance of 3B42V6, the 3B42V6 mean rainfall (MR), the gauged mean rainfall (MR), the NSE, FBI, and POD on different temporal scales of the two datasets from 107 stations and grids were computed firstly. Then the TCCs between each index and altitude, longitude, latitude, slope and aspect of 107 stations were calculated, as shown in Fig. 13. Compared to the Ccc (0.19 by 95 % significance test level), the factors of slope and aspect were mostly not through the significance test (in red); however, the other influence factors were almost all through the significance test (in blue). Therefore, the terrain elements of altitude, longitude and latitude were chosen as major influence factors; and the indices of NSE, FBI, and POD were used for validation.

The fitting degree of the two datasets on comprehensive rainfall amount (by NSE) and the rain event detection ability (by FBI and POD) of the 3B42V6 against gauges augmented with altitude, longitude, and latitude are presented in Fig. 14. The gauge stations were sorted along the x-axis by increasing altitude in (a), (b), and (c); by increasing longitude in (d), (e), and (f); and by increasing latitude in (g), (h), and (i). Gradually increasing trends emerged in the fitting degree of rainfall amount by NSE shown in Fig. 15a and in the rain event detection by FBI and POD shown in Fig. 15b and c of the 3B42V6 against gauges by a positive slope of trend lines with an augmentation of altitude. However, there were gradually decreasing trends appearing in the rainfall amount

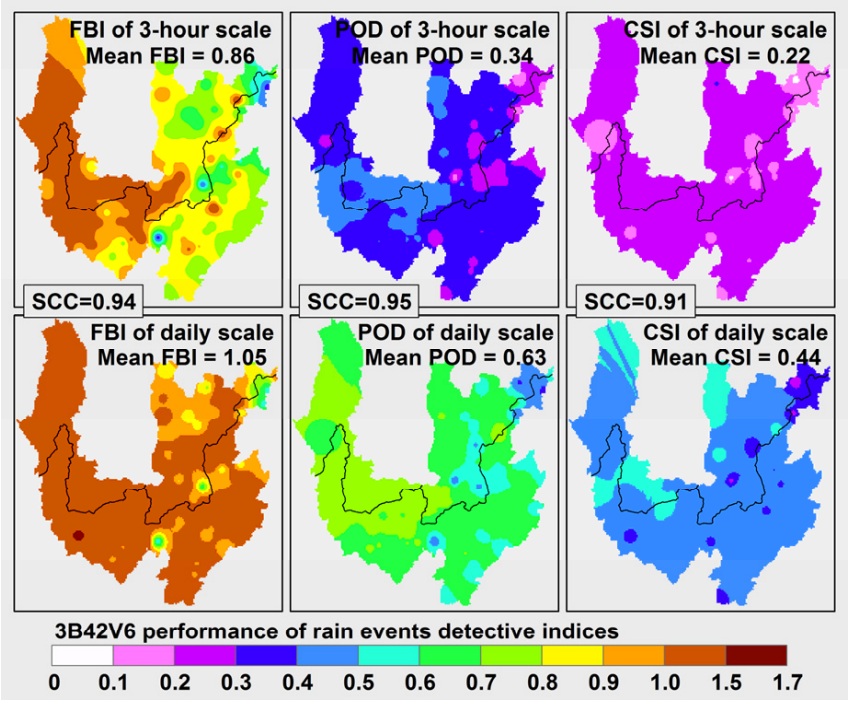

Fig. 11. Spatial patterns of rain event estimation indices on the 3 h and daily scales by the IDW interpolation method; each index computed by the 3B42V6 (107 grids) detection ability against gauged rain events from 107 stations over 2008–2010.

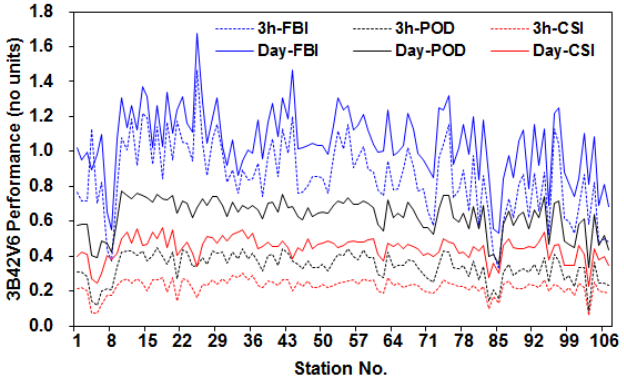

Fig. 12. Comparison of curves of 3B42V6 performance by rain event estimation indices on 3 h and daily scales over 2008–2010.

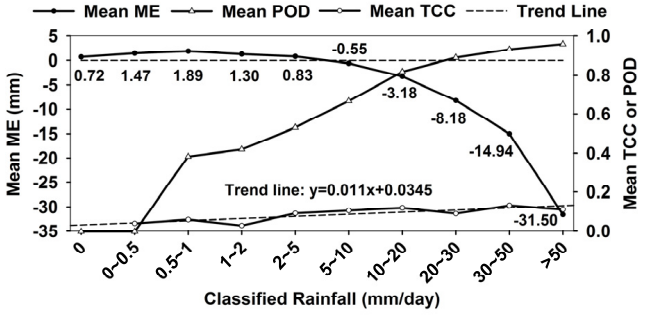

Fig. 13. Curves of variation trends for the 3B42V6 performance in rainfall mean error, temporal correlation coefficient, and probability of detection for rain events with the increasing of daily rainfall intensity.

fitting degree by NSE shown in Fig. 15d and g and rain event detection by FBI and POD shown in Fig. 15e-f and h-i of the 3B42V6 against gauges by a negative slope of trend lines with a longitude or a latitude augmentation. It is worth noting that the FBI values have a variation range from underestimation (FBI < 1.0) to overestimation (FBI > 1.0) as altitude increases, while changing from overestimation (FBI > 1.0) to underestimation (FBI < 1.0) as longitude or latitude increases.

4 Discussion

Validation of the 3B42V6 in the Jinsha River basin with alpine and gorge terrains revealed a different degree of consistencies and discrepancies on different spatio-temporal scales by gauges. Overall, there were satisfactory sum rainfall amounts and mean error estimates by the 3B42V6 on 3 h, daily, and monthly scales (Fig. 2). However, there were discrepancies in the mean rainfall amounts between the two datasets at fine temporal scales using NSE, e.g., a 3 h scale with a negative NSE value (Fig. 3). Therefore, further

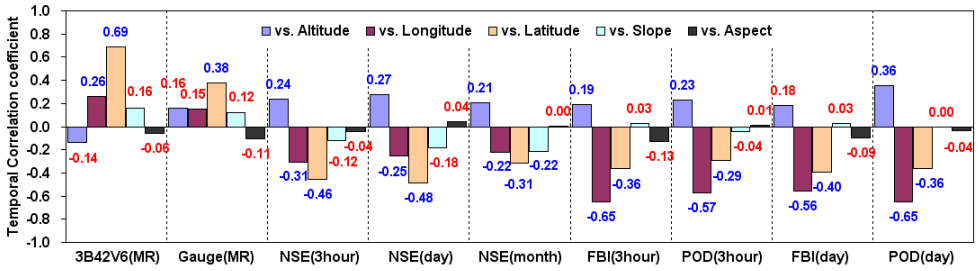

Fig. 14. The two-dimensional histograms of temporal correlation coefficient discrepancies of terrain factors between 3B42V6 (107 grids) and gauges (107 stations) on three temporal scales; 3B42V6(MR) and Gauge(MR) indicate the mean rainfall time series of the two datasets and had the same temporal correlation coefficient value for the three temporal scales. Those were not indicated on the temporal scale. The red numbers indicate the index through the 95 % significance test level and the blue numbers indicate the index not through the 95 % significance test level.

validation in single station of the 3B42V6 against gauges on rainfall amounts, rain event detection, seasonal error differences, performances in different gauged daily rainfall intensity and even terrain influence were of vital importance for using the 3B42V6 dataset in the research on the hydrological processes of the investigation area.

The correlation (by TCC) and rainfall amount fitting (by NSE) analyses of each station from the two datasets of rainfall time series stated in Sect. 3.2 proclaimed a better agreement with an augmentation of the temporal scales, and satisfactory rainfall amounts only fitting on the monthly scale with TCC having reached 0.9 and NSE having achieved 0.74 (Figs. 4 and 5). These conclusions had been verified by similar studies, such as those by Yong et al. (2010), Mansour (2011), Scheel et al. (2011) and Li et al. (2012), with an approximately equal TCC on monthly scale as 0.9 in the two datasets. There were acceptable TCC values, such as 0.59 (daily) and 0.34 (3 h), which were all through the 95 % significance test. However, a low NSE, such as 0.15 (daily) and −0.3 (3 h), the value of which is less than 0.5, means the accuracy was unsatisfactory (Moriasi et al., 2007) for the 3B42V6 on the daily or 3 h scales.

The mean month SCCs of the 3B42V6 against the gauges successively increased with the augmentation of the temporal scales. In addition, the mean month SCCs that were almost all invalid emerged during the dry months of the three temporal scales. However, valid SCCs emerged during the wet months of the three temporal scales. High SCC values also emerged in heavy rainfall time intervals of 3 h and daily scales (Figs. 6 and 8). That is, the 3B42V6 has satisfactory spatial distribution estimates during heavy rainfall time periods, but has unsatisfactory spatial distribution estimates during light rainfall time periods. Therefore, the spatial correlation should be allowed for the statistical significance of differences between these two datasets (Buarque et al., 2011; Clarke et al., 2011).

The rainfall amount relative bias analysis (by BIAS) demonstrated no regular distribution with over- and underestimates overall, and acceptable deviations during the wet seasons but disappointing deviations during the dry seasons (Fig. 9). The 3B42V6 was estimated by BIAS for approximately equal (± 10 %) at 37.4 % and for acceptable accuracy (± 25 %) at 80.4 % over 2008–2010 in the Jinsha River basin. These results differ from Bangladesh (Nepal), which are 38 % (19 %) and 72 % (57 %) for ± 10 % and ± 25 % in the monthly scale data, respectively (Islam and Uyeda, 2007; Islam et al., 2010).

The rain event detection ability of the 3B42V6 manifested a slight overestimation (FBI = 1.05) on the daily scale but an underestimation (FBI = 0.86) on the 3 h scale as a whole (Fig. 10), which is similar to Cusco, Peru, with an FBI at 0.97 on the daily scale (Scheel et al., 2011). The POD reached 0.34 on the 3 h scale and 0.63 on the daily scale (Fig. 10), which is analogous to Cusco, Peru, at 0.76 (Scheel et al., 2011) and the Laohahe Basin in China at 0.61 (Yong et al., 2010) on the daily scale. The rainfall variation trend estimates (by TCC) and rain event detection (by POD) of the 3B42V6 gradually increased with the augmentation of gauged daily rainfall intensity (Fig. 12). There was a daily rainfall threshold splitting overestimation of the 3B42V6 rainfall amounts of greater than 5.0 mm d^{-1} and underestimation of those of less than 5.0 mm d^{-1} (Fig. 12). This conclusion is similar to the research of Scheel et al. (2011) with a different threshold of 2.0 mm d^{-1}.

The terrain elements of altitude, longitude and latitude were the major factors affecting the 3B42V6 performance in the whole investigation area. It is worth mentioning that the slope and aspect did not show significance impacts because they are local, regime-dependent factors. In addition, the large inherent variation of rainfall also leads to the phenomenon, especially in alpine and gorge terrain. Overall, the comprehensive validation of terrain influence included rainfall amounts and rain event detection of the 3B42V6. The accuracy of 3B42V6 displayed improving trends with increasing of altitudes, and inversely, its accuracy displayed declining decreasing trends with increasing of longitudes or latitudes (Fig. 14).

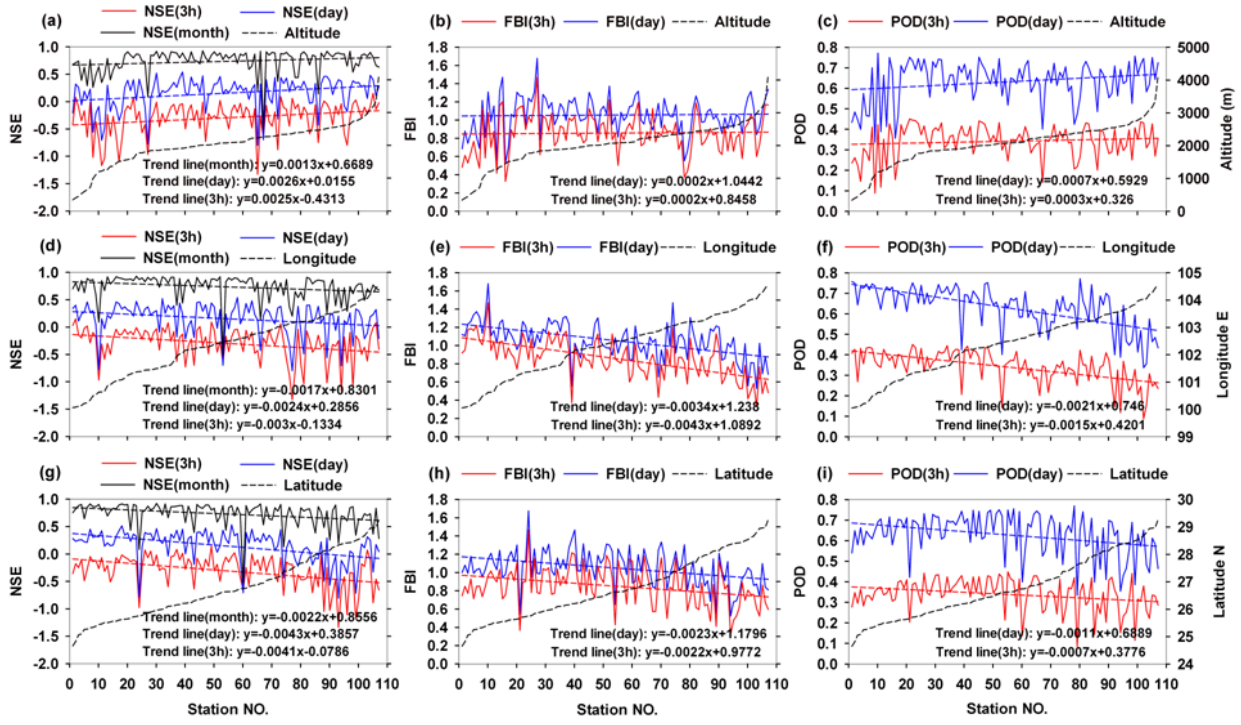

Fig. 15. Curves trends of the 3B42V6 (107 grids) detection ability for rainfall (by NSE) and rain events with augments of altitude, longitude and latitude. The gauge stations were sorted along the x-axis by increasing the altitude in **(a)**, **(b)**, and **(c)**; by increasing the longitude in **(d)**, **(e)**, and **(f)**; and by increasing the latitude in **(g)**, **(h)**, and **(i)**.

From what has been discussed above, there are acceptable consistencies of the 3B42V6 against the gauges on the daily and monthly scales. However, the 3B42V6 displayed disappointing accuracies on both rainfall amount estimates and rain event detection at the fine 3 h scale. In a further survey of the 3 h rainfall time series comparison between the two datasets from Fig. 3, the 3B42V6 rainfall time series revealed rain events in advance or at a lag against the gauges. This phenomenon may be a result of those discrepancies between the two datasets on the fine 3 h scale. Thus, for further inquiry the time asynchronism degree of the two datasets' rainfall time series, the 3B42V6 rainfall time series of 3 h scale given 3 h and 6 h in advance, and given 3 h and 6 h at a lag against the gauges, respectively, were analyzed. Fig. 15 displays the TCC discrepancies of the 3B42V6 with 3 h advance or 3 h lag against the gauges. The results illustrated that the 3B42V6 with 3 h advance still has an acceptable correlation against gauges (shown in blue; the TCC mean value averaged by 107 stations). Correspondingly, approximately half or more of the stations (66 in 2008, 44 in 2009, 60 in 2010) indicated higher TCC values than the original 3B42V6 against the gauges. However, the 3B42V6 rainfall time series with the 3 h lag had no invalid correlation against the gauges; similar conclusions emerged which were abbreviated in the 3B42V6 with 6 h advance or 6 h lag against the gauges. In other words, the 3B42V6 of the 3 h scale rainfall time series has slightly less than a 3 h lag against the gauged rainfall time series. This occurred because valid TCC values appeared between the original 3B42V6 and the 3B42V6 with 3 h advance against the gauges. Furthermore, these results confirmed that the two rainfall time series asynchronism should be a very important factor leading to disappointing performance of the 3B42V6 on the 3 h scale.

Of course, there are a variety of possible error sources for the 3B42V6. On one hand, the errors can be identified at the sensor and with the 3B42V6 product algorithm. The error analysis is complicated and it is difficult to track errors back to the input data. On the other hand, the TMPA version 7 and the upcoming Global Precipitation Measurement mission would have been programmed to improve this deficiency.

5 Conclusions

In conclusion, this study has comprehensively validated the 3B42V6 product on rainfall amount estimates, errors of seasonal differences, rain event detection, performance in different gauged daily rainfall intensities, and the terrain influence covered on the 3 h, daily and monthly temporal scales. The validation study showed that the 3B42V6 delivered acceptable estimates in sum rainfall. However, discrepancies

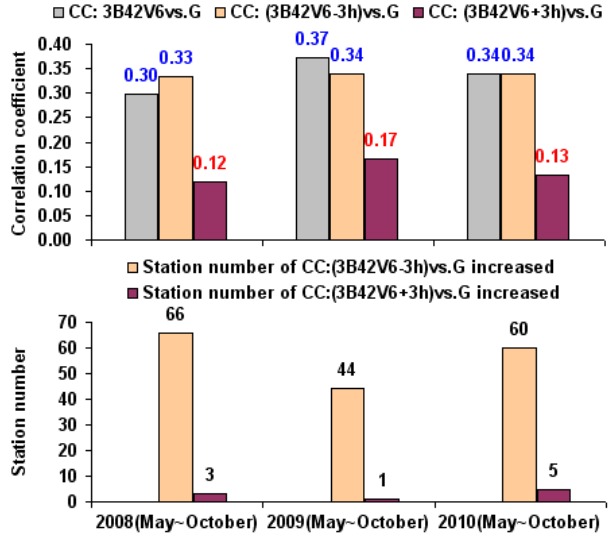

Fig. 16. The two-dimensional histograms display temporal correlation coefficient comparisons between 3B42V6, 3B42V6 with 3 h advance, and 3B42V6 with 3 h lag and gauged rainfall time series over May to October of 2008–2010. Correspondingly, station numbers of TCC were increased, which were computed by 3B42V6 with 3 h advance or lag against gauges comparing to the TCC values of the original 3B42V6 (107 grids) against gauges (107 stations). The red numbers indicate the TCC not through the 95 % significant test level; however the blue numbers indicate the TCC through the 95 % significant test level.

were seen in different time intervals; the 3B42V6 displayed increasing accuracy when temporal scales were augmented from 3 h to daily to monthly. Separately, the mean temporal correlation coefficient of the 3B42V6 against gauges reached 0.34 at the 3 h scale, 0.59 at the daily scale and 0.90 at the monthly temporal scale. The spatial distribution estimates of the 3B42V6 should be allowed for the statistical significance of differences between these two datasets. The rain events estimated by the mean probability of detection achieved 0.34 at the 3 h scale and 0.63 at the daily scale. A slight overestimation as a whole of the 3B42V6 existed with a mean relative bias of 3.94 %, and the stations of acceptable bias ($\pm$ 25 %) obtained 80.4 %. There is a threshold approximately equal to 5.0 mm d^{-1} in daily rainfall intensity, which split the 3B42V6 into overestimates (< 5.0 mm d^{-1}) and underestimates (> 5.0 mm d^{-1}). The terrain elements of altitude, longitude and latitude were the major factors for the 3B42V6 performance. Although there is a certain amount of discrepancy surrounding the 3B42V6, it has a great potential for the research on hydrologic processes. This is especially true at daily or larger temporal scales. As to fine temporal scales, such as those with the purpose of flood prediction, the 3 h scale dataset must be used. In this case, it is necessary to conduct adjustments or combine the 3B42V6 data with the gauge data from the investigation area.

Uncertainty of errors from different sources is inherent in the validation as shown by the ground station gauge data. A method to quantify the uncertainty in the TMPA validation results, which arises from uncertainties in the gauge, is still a challenge for the scientific community. While the aim of TMPA products would be widely used in the research of regional hydrologic processes, the following activities are proposed or are already being planned by several agencies and programs. These activities are likely to be programmed to improve the noted deficiencies. They include: combining the satellite dataset with the gauge data, especially for fine spatio-temporal resolutions, version 7 products of the TMPA, and the Global Precipitation Measurement mission for which the Core satellite is to be launched.

Acknowledgements. The authors would like to acknowledge the Presidency of the Hydrologic Data Center of the Three Gorges Project Corporation in China for providing the rain-gauge data. The TMPA product, which was acquired from the website at http://trmm.gsfc.nasa.gov, is an international project jointly sponsored by the Japan Aerospace Exploration Agency (JAXA) and the US National Aeronautics Space Administration (NASA), Office of Earth Science. This study is supported by the Action Plan for the West Development of Chinese Academy of Sciences (CAS), (Grant No. KZCX2-XB3-08). All of these resources are highly appreciated.

Edited by: A. Mugnai
Reviewed by: two anonymous referees

References

Asadullah, A., Mcintyre, N., and Kigobe, M.: Evaluation of five satellite products for estimation of rainfall over Uganda, Hydrol. Sci. J., 53, 1137–1150, 2008.

Brown, J. E. M.: An analysis of the performance of hybrid infrared and microwave satellite precipitation algorithms over India and adjacent regions, Remote Sens. Environ., 101, 63–81, 2006.

Buarque, D. C., De Paiva, R. C. D., Clarke, R. T., and Mendes, C. a. B.: A comparison of Amazon rainfall characteristics derived from TRMM, CMORPH and the Brazilian national rain gauge network, J. Geophys. Res.-Atmos., 116, 19105–19105, doi:10.1029/2011JD016060, 2011.

Chen, H., Yuan, W. H., and Li, J.: A Possible Cause for Different Diurnal Variations of Warm Season Rainfall as Shown in Station Observations and TRMM 3B42 Data over the Southeastern Tibetan Plateau, Adv. Atmos. Sci., 29, 193–200, 2012.

Chokngamwong, R. and Chiu, L.: Thailand Daily Rainfall and Comparison with TRMM Products. J. Hydrometeor., 9, 256–266, doi::http://dx.doi.org/10.1175/2007JHM876.1, 2008.

Clarke, R. T., Buarque, D. C., De Paiva, R. C. D., and Collischonn, W.: Issues of spatial correlation arising from the use of TRMM rainfall estimates in the Brazilian Amazon, Water Resour. Res., 47, W05539, doi:10.1029/2010WR010334, 2011.

Dai, A., Iin, X., and Hsu, K.: Thefrequeney, intensity, and diurnal cycle of precipitation in surfaee and satellite observations over low-and mid-latitudes, Clim. Dynam., 29, 727–744, 2007.

Ebert, E. E., Janowiak, J. E., and Kidd, C.: Comparison of near-real-time precipitation estimates from satellite observations and numerical models, Bull. Am. Meteorol. Soc., 88, 47–64, doi:10.1175/BAMS-88-1-47, 2007.

Gu, H., Yu, Z. B., Yang, C. G., Liang, C., Wang, W., and Ju, Q.: Application of Satellite Radar Observed Precipitation to Accuracy Analysis in Yangtze River Basin, Water Resour. Power, 28, 3–6, 2010.

Huffman, G., Adler, R., Bolvin, D., Gu, G., Nelkin, E., Bowman, K., Hong, Y., Stocker, E., and Wolff, D.: The TRMM Multisatellite Precipitation Analysis (TCMA): Quasi-global, multiyear, combined-sensor precipitation estimates at fine scales, J. Hydrometeorol., 8, 38–55, doi:10.1175/JHM560.1, 2007.

Islam, M. N. and Uyeda, H.: Use of TRMM in determining the climatic characteristics of rainfall over Bangladesh, Remote Sens. Environ., 108, 264–276, 2007.

Islam, M. N., Das, S., and Uyeda, H.: Calibration of TRMM derived rainfall over Nepal during 1998-2007, Open Atmos. Sci. J., 4, 12–23, doi:10.2174/1874282301004010012, 2010.

Jia, S., Zhu, W. B., Lv, A. F., and Yan, T. T. A statistical spatial downscaling algorithm of TRMM precipitation based on NDVI and DEM in the Qaidam Basin of China, Remote Sens. Environ., 115, 3069–3079, 2011.

Li, X. H., Zhang, Q., and Xu, C. Y.: Suitability of the TRMM satellite rainfalls in driving a distributed hydrological model for water balance computations in Xinjiang catchment, Poyang lake basin, J. Hydrol., 426–427, 28–38, 2012.

Liu, J. F., Chen, R. S. and Han, C. T.: Evaluating TRMM multisatellite precipitation analysis using gauge precipitation and MODIS snow-cover products, Adv. Water Sci., 22, 447–454, 2011.

Luo, S., Miao, J. F., and Niu, T.: The rain TRMM products 3B42 and stations in China of the regional data analysis, Meteorological Monthly, 37, 1081–1090, 2011.

Mansour, A.: Calibration of TRMM rainfall climatology over Saudi Arabia during 1998–2009, Atmos. Res., 99, 400–414, 2011.

Montero-Martínez, G., Zarraluqui-Such, V., and García-García, F.: Evaluation of 2B31 TRMM-product rain estimates for single precipitation events over a region with complex topographic features, J. Geophys. Res., 117, D02101, doi:10.1029/2011JD016280, 2012.

Moriasi, D. N., Arnold, J. G., Van Liew, M. W., Bingner, R. L., Harmel, R. D., and Veith, T. L.: Model evaluation guidelines for systematic quantification of accuracy in watershed simulations, Trans. ASABE, 50, 885–900, 2007.

Scheel, M. L. M., Rohrer, M., Huggel, Ch., Santos Villar, D., Silvestre, E., and Huffman, G. J.: Evaluation of TRMM Multisatellite Precipitation Analysis (TMPA) performance in the Central Andes region and its dependency on spatial and temporal resolution, Hydrol. Earth Syst. Sci., 15, 2649–2663, doi:10.5194/hess-15-2649-2011, 2011.

Shen, H. Y. and Yang, W. F.: Jinshajiang river basin for the analysis of characteristics of the heavy rain, Chinese J. Water Resour. Res., 28, 39–41, 2007.

Sorooshian, S., Lawford, R., Try, P., Rossow, W., Roads, J., Polcher, J., Sommeria, G., and Schiffer, R.: Water and energy cycles: Investigating the links, WMO Bull., 54, 58–64, 2005.

Su, F. G., Hong Y., and Lettenmaier D. P. : Evaluation of TRMM Multisatellite Precipitation Analysis (TMPA) and Its Utility in Hydrologic Prediction in the La Plata Basin, J. Hydrometeorol., 9, 622–640, 2008.

Tobin, K. J. and Bennett M. E.: Adjusting Satellite Precipitation Data to Facilitate Hydrologic Modeling, J. Hydrometeorol., 11, 966–978, doi:10.1175/2010JHM1206.1, 2010.

Vera, T., Rodrigo, R., Mauricio, Z.-B., Vincenzo, L., and Ad, D. R.: Validation of Satellite-Based Precipitation Products over Sparsely Gauged African River Basins, J. Hydrometeorol., 13, 1760–1783, 2012.

Yong, B., Ren, L. L., Hong, Y., Wang, J.-H., Gourley, J. J., Jiang, S. H., Chen, X., and Wang, W.: Hydrologic evaluation of Multisatellite Precipitation Analysis standard precipitation products in basins beyond its inclined latitude band:A case study in Laohahe basin, China, Water Resour. Res., 46, W07542, doi:10.1029/2009WR008965, 2010.

Yuan, W., Li, J., Chen, H. M., and Yu, R. C. Intercomparison of summer rainfall diurnal features between station rain gauge data and TRMM 3B42 product over central eastern China, Int. J. Climatol., 32, 1690–1696, doi:10.1002/joc.2384, 2012.

Zhou, T., Yu, R., and Chen, H.: Summer Preeipitation frequeney, intensity, and diurnal cycle over China: Aeornparison of satellite data with rain gauge obsevations, J. Climate, 21, 3997–4010, 2008.